Eur. Phys. J. C (2024) 84:1098
https://doi.org/10.1140/epjc/s10052-024-13426-w

THE EUROPEAN PHYSICAL JOURNAL C

Regular Article - Theoretical Physics

Investigating new aspects of Bocharova–Bronnikov–Melnikov–Bekenstein spacetime: ionized thin accretion disk model

Bobur Turimov[1,2,3,a], **Akbar Davlataliev**[1,b], **Yusuf Usmanov**[4], **Shavkat Karshiboev**[5], **Pulat Tadjimuratov**[6]

[1] Institute of Fundamental and Applied Research, National Research University TIIAME, Kori Niyoziy 39, Tashkent 100000, Uzbekistan
[2] University of Tashkent for Applied Sciences, Str. Gavhar 1, Tashkent 100149, Uzbekistan
[3] Shahrisabz State Pedagogical Institute, Shahrisabz Str. 10, Shahrisabz 181301, Uzbekistan
[4] National Research University TIIAME, Kori Niyoziy 39, Tashkent 100000, Uzbekistan
[5] Uzbek-Finnish Pedagogical Institute, Spitamen Shokh St. 166, Samarkand 140100, Uzbekistan
[6] Central Asian University, Milliy Bog St. 264, Tashkent 111221, Uzbekistan

Received: 14 August 2024 / Accepted: 25 September 2024

Abstract Accretion processes near black hole candidates are associated with the high-energy emission of radiation from relativistic particles and outflows. It is widely believed that the magnetic field plays a crucial role in explaining these high-energy processes near these astrophysical sources. In this work, we analyze thin accretion disks in the Bocharova–Bronnikov–Melnikov–Bekenstein (BBMB) spacetime framework using the Novikov–Thorne model. Our study examines the thermal and optical characteristics of these disks, including their emission rate and luminosity in the specified spacetime. Later, we extend the Novikov–Thorne model to ionized thin accretion disk. We propose that the black hole is embedded in an asymptotically uniform magnetic field. We investigate the dynamics of charged particles near a weakly magnetized black hole. Our findings show that, in the presence of a magnetic field, the radius of the marginally stable circular orbit (MSCO) for a charged particle is close to the black hole's horizon. The orbital velocity of the charged particle, as measured by a local observer, has been computed in the presence of the external magnetic field. We also present an analytical expression for the four-acceleration of the charged particle orbiting around black holes. Finally, we determine the intensity of the radiation emitted by the accelerating relativistic charged particle orbiting the magnetized black hole.

1 Introduction

The observation of astrophysical black holes, such as supermassive black holes (SMBHs) and stellar black holes, has sparked renewed interest in studying the behavior of charged particles in the presence of external electromagnetic fields around these black holes. It is generally recognized that magnetic fields play a crucial role in driving the most energetic processes near supermassive black holes at the centers of galaxies, serving as a "feeder" by capturing dust close to the galaxy's core. Charged particle motion around the black hole in the presence of the external magnetic field has been extensively studied in [1–9]. The effect of the radiation reaction on charged particle motion around back hole is investigated in [10–17].

The recent detection of the shadow of the supermassive black hole (SMBH) candidate in the galaxy M87 [18] has sparked a renewed interest in exploring the characteristics of extreme gravitational compact objects (see, for instance, [19–21]). This exploration involves developing methods to derive information about the object's mass and spin from observations while imposing limits on additional parameters associated with black hole mimickers, such as NUT charges [22] or mass quadrupole moments [23]. Observational data, including the orbital motion of stars near an SMBH candidate, spectra from accretion disks around the compact object, and the object's 'shadow'-like that of the SMBH candidate in M87-can provide valuable insights. For instance, the mass of the SMBH candidate at the Milky Way's center can be inferred from the Newtonian motion of S2 stars observed in infrared wavelengths [24,25]. Similarly, the inner edge

[a] e-mail: bturimov@astrin.uz
[b] e-mail: akbar@astrin.uz (corresponding author)

Published online: 23 October 2024

of the SMBH candidate's shadow in M87 can reveal information about the central object's angular momentum [26]. Additional parameters of gravitational compact objects can be estimated by analyzing the thermal spectrum of accretion disks and fluorescent iron lines in low-mass X-ray binaries (LMXB) [27,28]. Combining various observational techniques and methods can, in principle, help constrain these parameters and elucidate the geometry surrounding the compact object.

For example, the mass of the SMBH candidate at the center of the Milky Way galaxy can be determined through the Newtonian motion of S2 stars observed in infrared (IR) wavelengths. Similarly, the inner edge of the shadow of the SMBH candidate in M87 provides insights into the angular momentum of the central object. Other parameters of gravitational compact objects can be estimated through detailed analyses of the thermal spectra of accretion disks and fluorescent iron lines in low-mass X-ray binaries (LMXBs). By combining different observations and methods, it is possible to constrain additional parameters and understand the geometry surrounding the compact object.

An accretion disk is a complex formation created by diffuse matter orbiting a massive central compact object. In this environment, gravitational and frictional forces compress and heat the matter, resulting in the emission of highly energetic electromagnetic radiation. The frequency of this radiation is heavily influenced by the central object's total mass. When the accretion rate is sub-Eddington and the opacity is extremely high, a geometrically thin accretion disk forms. This disk is thin in the vertical direction and exhibits a disk-like shape in the orbital plane. The radiation pressure within the disk can be considered negligible, causing the gas to spiral tightly towards the central object, closely approximating free Keplerian circular orbits. Thin disks are relatively luminous and produce thermal electromagnetic black body radiation. Building on the foundational work by Shakura and Sunyaev [29] on thin accretion disks, the key characteristics of these disks have been further developed by various researchers (see, for example, [30,31]).

A general relativistic approach is essential for describing the inner regions of an accretion disk around a black hole. This framework was initially developed by Novikov, Page, and Thorne [32–34]. Luminet [35] was the first to create simulated optical images of an accretion disk around a black hole, revealing that even a symmetrically structured black hole can produce asymmetric images. This asymmetry arises because the Doppler beaming effect, which is crucial for maintaining centrifugal equilibrium in the strong gravitational field near the black hole, causes a significant Doppler redshift on the disk's receding side and a strong blueshift on the approaching side. Additionally, light bending distorts the appearance of the disk, making it seem as though it is not obscured by the black hole. Recent simulations by Mizuno et al. [36] using fully relativistic models have been developed to image various massive candidates for the central compact object in M87, aiming to constrain the potential existence of exotic compact objects. The properties of the thin accretion disk in various spacetime has been studied in [37–58]. In this paper, we examine a thin accretion disk within the BBMB spacetime [59,60].

The article is organized as follows. In Sect. 2 we consider the thermal properties of thin accretion disks in the around the BBMB black hole using the Novikov–Thorne model [32]. In particular, we simulate the thermal spectrum of the disk. In Sect. 3, we study the thermal properties of ionized accretion disk. Finally, the last Sect. 4 summarizes the main results and their potential implications for astrophysical black hole candidates.

2 Novokov–Thorne thin accretion disk model

We now consider the thermal properties of thin accretion disks using the framework originally developed by Novikov and Thorne [32], extending the model to the BBMB-spacetime. The Novikov–Thorne model describes an accretion disk around a massive black hole based on general relativity principles, detailing how matter spirals into a black hole. This model, which incorporates the effects of general relativity, can also be applied to the BBMB spacetime. General relativity and alternative theory of gravity explain the curvature of spacetime around massive objects, leading to phenomena such as gravitational time dilation and frame-dragging in the vicinity of black holes.

Accretion around a black hole or extremely compact object occurs in the region $r > r_{\rm ms}$, where $r_{\rm ms}$ is the radius of the ISCO of test particles. The radius of the marginally stable orbit serves as the inner edge of the thin accretion disk $r_{\rm in} = r_{\rm ms}$, while the outer edge $r_{\rm out}$ can be freely chosen. For our calculations, we have set $r_{\rm out} = 30M_* \gg r_{\rm in}$. As particles fall from rest at infinity and accrete onto the central object, they heat up, converting gravitational energy into radiation that is then emitted into space.

The Novikov–Thorne model has been influential in astrophysics, used to interpret observations of black hole X-ray binaries and active galactic nuclei (AGN). It provides a theoretical framework for understanding matter accretion onto black holes and the energy release as radiation, which can be used to study these extreme cosmic objects. To model the thin accretion disk, the following assumptions are made:

– Matter in the accretion disk loses energy as it spirals inward towards the central object due to friction and gravitational forces, resulting in the emission of radiation, primarily X-rays and other high-energy photons.

- The accretion disk is a flattened, rotating structure composed of gas, dust, and other matter. As matter falls inward, it follows nearly circular orbits, gradually losing angular momentum and spiraling closer to the black hole. The disk is assumed to be geometrically thin and optically thick, meaning the radial extension $\Delta r = r_{\rm out} - r_{\rm in}$ is much larger than its thickness $h << \Delta r$.
- According to the Novikov–Thorne model, there is an innermost stable circular orbit (ISCO) where matter can orbit the black hole or exotic object without rapidly falling in. The radius of this orbit depends on the black hole's mass and angular momentum. Inside the ISCO, matter plunges rapidly into the central object.
- The innermost part of the accretion disk is very close to the black hole's event horizon, beyond which nothing can escape the black hole's gravitational pull. Radiation emitted near the event horizon is highly redshifted, making detection difficult.
- The motion of gas particles in the disk approximately follows circular Keplerian orbits, well-described by test particles on circular orbits.
- The torque near the inner edge of the accretion disk is negligible.
- The mass accretion rate of the thin disk is constant and less than the Eddington mass rate, specifically, $\dot{\mathscr{M}} \simeq (0.03 - 0.5)\dot{\mathscr{M}}_{\rm Edd}$, where the Eddington mass rate is defined as

$$\dot{\mathscr{M}}_{\rm Edd} = \frac{4\pi G M m_p}{c\sigma_T}$$

  with M as the mass of the gravitational object, m_p as the proton mass, and σ_T as the Thompson cross-section for the electron. In solar mass units, $\dot{\mathscr{M}}_{\rm Edd} \simeq 2.33 \times 10^{18}\,(M/M_\odot)\ {\rm g}\cdot{\rm s}^{-1}$.
- The model predicts that the radiation emitted by the accretion disk will have a characteristic spectrum, influenced by factors such as the black hole's mass and spin, with a distinctive peak in the X-ray part of the electromagnetic spectrum.

Now, we focus on the motion of massive particles orbiting around a spherically symmetric black hole. To describe particles on accretion disks, we restrict our attention to circular orbits in the equatorial plane, so the particle's four-velocity is given by $\dot{x}^\alpha = (\dot{t}, 0, 0, \dot{\phi})$. The explicit expressions for the constants of motion, which are the specific energy $\mathscr{E}$, specific angular momentum $\mathscr{L}$, and angular velocity Ω of test particles at a radius r, as measured by a distant observer, can be obtained from:

$$\mathscr{E} = -\frac{g_{tt}}{\sqrt{-g_{tt} - \Omega^2 g_{\phi\phi}}}\,, \tag{1}$$

$$\mathscr{L} = \frac{g_{\phi\phi}\Omega}{\sqrt{-g_{tt} - \Omega^2 g_{\phi\phi}}}\,, \tag{2}$$

$$\Omega = \frac{d\phi}{dt} = \sqrt{-\frac{\partial_r g_{tt}}{\partial_r g_{\phi\phi}}}\,. \tag{3}$$

where g_{tt} and $g_{\phi\phi}$ are temporal and azimuthal components of the metric tensor.

From the conservation laws of energy-momentum ($\nabla_\mu T^{\mu\nu} = 0$) and continuity equation ($\nabla_\mu J^\mu = 0$) for matter containing on disk, the radiant energy flux of the accretion disk can be derived as [33,34]

$$F(r) = -\frac{\dot{\mathscr{M}}}{4\pi\sqrt{-\tilde{g}}}\frac{\Omega'}{(\mathscr{E} - \Omega\mathscr{L})^2}\int_{r_{\rm ms}}^{r} dr(\mathscr{E} - \Omega\mathscr{L})\mathscr{L}'\,, \tag{4}$$

where a prime ($'$) denotes the derivative with respect to radial coordinate r and $\tilde{g} = \sqrt{-g_{tt}g_{rr}g_{\phi\phi}}$ is the determinant of the metric tensor in the equatorial plane. Since the accretion disk is assumed to be in local thermal equilibrium, the disk emission is black-body radiation, for which the Stefan-Boltzmann law is applicable and the temperature of the disk is determined as

$$T(r) = \sqrt[4]{\frac{F(r)}{\sigma}}\,. \tag{5}$$

where σ is the Stephan-Bolztman constant.

Another important aspect of mass accretion activity is the energy efficiency ε, which is determined by the specific energy of a particle at the marginally stable orbit $r_{\rm ms}$ when all the radiated photons can escape to infinity. This efficiency ε (which must be non-negative) indicates how effectively the central object converts rest mass into outgoing radiation. The accretion efficiency is given by: $\varepsilon = 1 - \mathscr{E}_{\rm ms}$.

The spectral luminosity of the radiation can be determined using the following expression

$$L(\nu) = \frac{8\pi h\cos i}{c^2}\int_{r_{\rm in}}^{r_{\rm out}}\int_0^{2\pi}\frac{\nu_e^3 r dr d\phi}{\exp\left(\frac{h\nu_e}{k_B T}\right) - 1}\,, \tag{6}$$

where i represents the inclination angle of the accretion disk, $r_{\rm in}$ is the inner edge, and $r_{\rm out}$ is the outer edge of the disk. For simplicity, one can choose $r_i = r_{\rm ms}$ and $r_{\rm out} \to \infty$, since at asymptotic infinity $r \to \infty$, the flux over the disk surface diminishes, as it does for any astronomical object. The frequency ν is measured by a distant observer while ν_e is the frequency of photons emitted from the accretion disk. These two frequencies are related to each other through the red-shift factor, i.e. $g = \nu_e/\nu$, which can be expressed as

$$g = \frac{1 + \Omega r\sin\phi\sin i}{\sqrt{-g_{tt} - \Omega^2 g_{\phi\phi}}}\,. \tag{7}$$

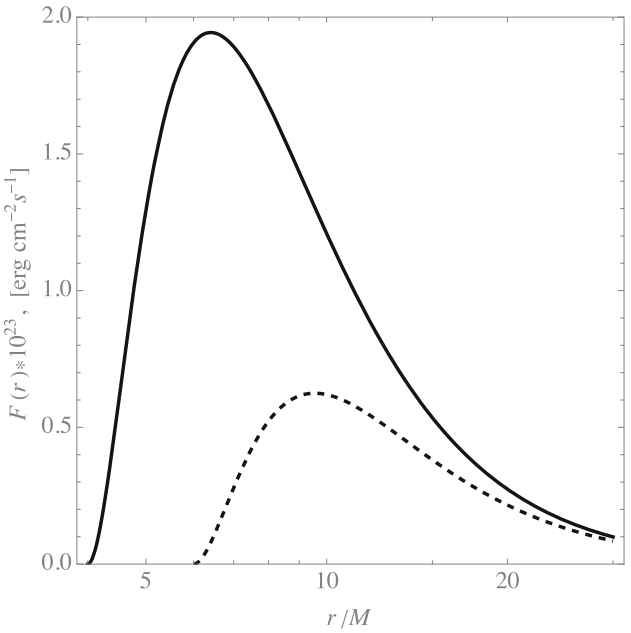

Fig. 1 The profile of the radiant energy flux of the thin disk in the BBMB spacetime (solid line) and in the Schwarzschild spacetime (dashed line) for the value of accretion rate $\dot{\mathscr{M}} = 0.1\dot{\mathscr{M}}_{\rm Edd}$

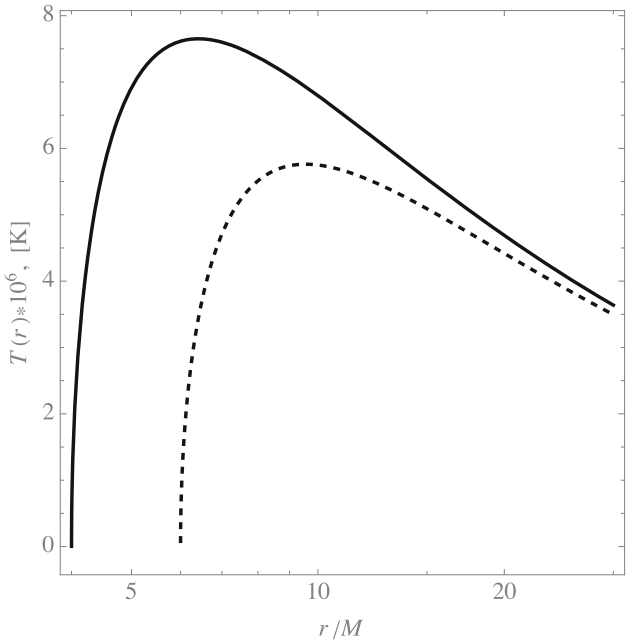

Fig. 2 Temperature profile of the thin disk in the BBMB spacetime (solid line) and in the Schwarzschild spacetime (dashed line) for the value of accretion rate $\dot{\mathscr{M}} = 0.1\dot{\mathscr{M}}_{\rm Edd}$

Now we consider the thin accretion disk model in the BBMB spacetime. We first start from calculating of radiant energy flux from the surface thin disk. Recalling Eq. (4) the radiant energy flux emitted by the disk surrounded the BBMB black hole can be expressed as

$$F(r) = \frac{\dot{\mathscr{M}}c^2}{8\pi M^2}\left(\frac{M}{r}\right)^3\left(1-\frac{M}{r}\right)^{-3/2}\left(\frac{3r-4M}{r-2M}\right) \times\left[\sqrt{1-\frac{M}{r}}+\sqrt{\frac{M}{r}}\ln\sqrt{\frac{\sqrt{r-M}+\sqrt{M}}{\sqrt{r-M}-\sqrt{M}}\frac{\sqrt{3}-1}{\sqrt{3}+1}} -\sqrt{\frac{3M}{r}}+\frac{2\pi}{3}\sqrt{\frac{M}{r}}-2\sqrt{\frac{M}{r}}\tan^{-1}\sqrt{1-\frac{M}{r}}\right], \tag{8}$$

while in the Schwarzschild spacetime, it reads as follows [35,57]

$$F(r) = \frac{3.\dot{\mathscr{M}}c^2}{8\pi M^2}\left(\frac{M}{r}\right)^3\left(1-\frac{3M}{r}\right)^{-1} \times\left[1-\sqrt{\frac{6M}{r}}+\sqrt{\frac{3M}{r}}\ln\sqrt{\frac{\sqrt{r}+\sqrt{3M}}{\sqrt{r}-\sqrt{3M}}\frac{\sqrt{2}-1}{\sqrt{2}+1}}\right]. \tag{9}$$

Figure 1 shows how the radiant energy flux varies radially across the disk in both BBMB and Schwarzschild spacetimes. It's important to note that the marginally stable circular orbits differ between these spacetimes, with $r_{\rm ms} = 4M$ in the BBMB spacetime and $r_{\rm ms} = 6M$ in the Schwarzschild spacetime. As one can see from Fig. 1, the inner edges of the disks in these spacetimes are different. However, the asymptotic behavior of the radiant energy flux is similar in both cases. On the other hand, numerical calculations showed that the maximum value of the radiant energy flux in the BBMB spacetime is more than three times greater than that in the Schwarzschild spacetime. Using Eq. (5) the radial distribution of the disk temperature can be illustrated in both BBMB and Schwazrschild spacetimes as shown in Fig. 2. The curves exhibit similar behavior with variations in the intensity parameter of the SBR, comparable to the flux.

As we mentioned before that one of the important features of the accretion disk is related to the radiative energy efficiency of the disk which is independent of the coordinate system. It can be expressed as the difference between the specific energies of the particle at infinity and at the marginally stable circular orbit. Our analytical and numerical calculations showed that energy efficiency in the BBMB spacetime is $\eta = 1 - 3\sqrt{6}/8 \simeq 0.08$ ($\sim 8\%$), however, in the Schwarzschild spacetime it is $\eta = 1 - \sqrt{8/9} \simeq 0.06$ ($\sim 6\%$).

Figure 3 presents the total spectral luminosity emitted by a thin accretion disk in the for fixed inclination angle $i = \pi/6$. It is important to note that at $\chi = \pi/2$, the spectral luminosity will be zero due to the cos χ factor in Eq. (6). As illustrated in each panel of Fig. 3, there is negligible variation in the spectra across different cases in the low-frequency region (covering infrared (IR), optical, and ultraviolet (UV) bands). However,

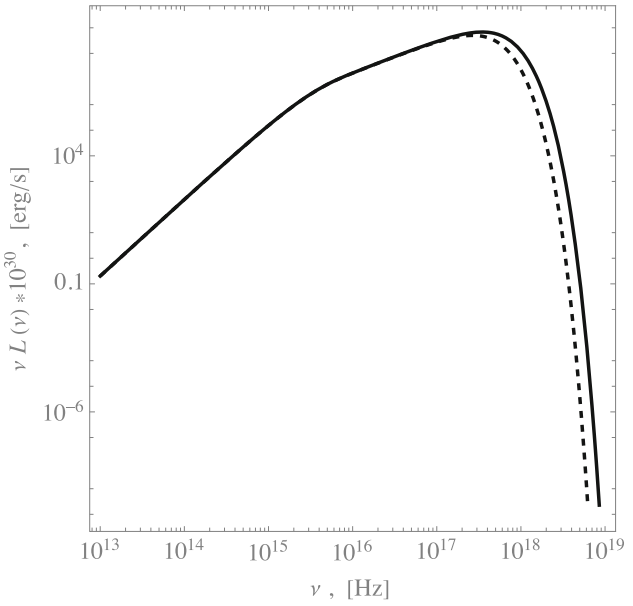

Fig. 3 The spectral luminosity of the thin disk as a function of frequency in the BBMB (solid) and Schwarzschild (dashed) spacetimes for the value of accretion rate $\dot{\mathscr{M}} = 0.1\dot{\mathscr{M}}_{\rm Edd}$

in the high-frequency region, particularly the X-ray band, a significant difference between each curve is observable. Additionally, the frequency corresponding to the maximum luminosity is influenced by an external term in the metric function, implying that such observations could potentially be used to test the nature of the geometry.

3 Ionized thin accretion disk model

Here we discuss simple this accretion disk in the BBMB spacetime. In general, it is known that total charge of the accretion disk is neutral. However we assume that matter in the accretion contains from mainly charged particles. Now one can study the charged particle motion in the curved spacetime in the presence of the external external magnetic field. The Lagrangian for test particle of mass m and charge q can be written as

$$L = \frac{1}{2} g_{\alpha\beta}\dot{x}^\alpha \dot{x}^\beta + \frac{q}{m} A_\alpha \dot{x}^\alpha \,, \qquad \dot{x}^\alpha = \frac{dx^\alpha}{ds} \,, \tag{10}$$

where A_α is the vector potential of the electromagnetic field. Equation of motion for charged particle can be derived as

$$\ddot{x}^\mu + \Gamma^\mu_{\alpha\beta}\dot{x}^\alpha \dot{x}^\beta = \frac{q}{m} F^\alpha_\beta \dot{x}^\beta \,, \qquad F_{\alpha\beta} = \partial_\alpha A_\beta - \partial_\beta A_\alpha \,. \tag{11}$$

Constants of motion, namely, the specific energy, $\mathscr{E}$ and specific angular momentum, $\mathscr{L}$, of charged particle can be expressed as

$$p_t = \frac{\partial L}{\partial \dot{t}} = g_{tt}\dot{t} + \frac{q}{m} A_t = -\mathscr{E} \,, \tag{12}$$

$$p_\phi = \frac{\partial L}{\partial \dot{\phi}} = g_{\phi\phi}\dot{\phi} + \frac{q}{m} A_\phi = \mathscr{L} \,. \tag{13}$$

We consider circular motion of particle in the equatorial plane with four-velocity of $\dot{x}^\alpha = (\dot{t}, 0, 0, \dot{\phi})$. Then specific energy and specific angular momentum of particle can be found as

$$\mathscr{E} = -\frac{g_{tt}}{\sqrt{-g_{tt} - \Omega^2 g_{\phi\phi}}} - \frac{q}{m} A_t, \tag{14}$$

$$\mathscr{L} = \frac{g_{\phi\phi}}{\sqrt{-g_{tt} - \Omega^2 g_{\phi\phi}}} - \frac{q}{m} A_\phi \,, \tag{15}$$

and the angular velocity of test particle Ω is found from the following equation:

$$\frac{\partial_r g_{tt} + \Omega^2 \partial_r g_{\phi\phi}}{\sqrt{-g_{tt} - \Omega^2 g_{\phi\phi}}} = -\frac{2q}{m} \left(F_{rt} + \Omega F_{r\phi}\right), \tag{16}$$

which can be obtained from Eq. (11).

3.1 Magnetic field configuration

In realistic astrophysical scenarios, the magnetic field configuration near a gravitational compact object is highly complex. However, for simplicity, one can consider an analytical expression for the magnetic field. A straightforward approach is provided by Wald [61]. According to this approach, the black hole is placed in an asymptotically uniform magnetic field, and the exact analytical expression for the vector potential in Schwarzschild space is given as

$$A_\phi = \frac{1}{2} B r^2 \sin^2\theta \,, \tag{17}$$

where B is the magnetic field strength. Note that the expression (17) is independent of the mass of the Schwarzschild black hole and fully satisfied the Maxwell equations in curved spacetime is given as

$$\nabla_\alpha F^{\alpha\beta} = 0 \,. \tag{18}$$

Similarly, in the background of the BBMB spacetime Maxwell's equation can be analytically solved and expression for the vector potential can be found as

$$A_\phi = \frac{1}{2} B \psi(r) \sin^2\theta \,, \tag{19}$$

which is similar to the solution in the Schwarzschild spacetime in (17), however new radial function $\psi(r)$ substituted instead of r^2. Now inserting Eq. (19) into (18), one can obtain

$$r^2 \left[f \psi'(r)\right]' - 2\psi(r) = 0 \,, \tag{20}$$

where a prime denotes the derivative with respect to radial coordinate. The solution to Eq. (20) can be expressed as $\psi(r) = C(r^2 - M^2)$, where C is constant of integration that should be equal to 1. Finally, the exact analytical solution of Maxwell equation for the vector potential near the BBMB black hole can be found as

$$A_\phi = \frac{1}{2} B \left(r^2 - M^2\right) \sin^2\theta \,, \tag{21}$$

non-zero components of the electromagnetic field tensor are $F_{r\phi} = Br\sin^2\theta$ and $F_{\theta\phi} = B(r^2 - M^2)\sin\theta\cos\theta$, while non-zero components of the magnetic field measured by a proper observer read

$$B^{\hat{r}} = B\left(1 - \frac{M^2}{r^2}\right)\cos\theta \,, \qquad B^{\hat{\theta}} = B\left(1 - \frac{M}{r}\right)\sin\theta \,. \tag{22}$$

To study the magnetic field configuration in the vicinity of the black hole, we can analyze the magnetic field lines represented by considering the following the equation $A_\phi =$ const. In Fig. 4, we provide a visualization of the magnetic field lines near the BBMB black hole. It is apparent that due to additional term in the metric function the magnetic field lines extend outward from the black hole in a more uniform manner.

3.2 Charged particle motion

Now we consider charged particle in the BBMB spacetime in the presence of the asymptotic uniform magnetic field. Using the normalization of the four-velocity $\dot{x}_\alpha \dot{x}^\alpha = -1$, equation of the radial motion can be obtained as follows

$$\dot{r}^2 = \mathscr{E}^2 - V(r) \,, \tag{23}$$

where the effective potential reads

$$V(r) = \left(1 - \frac{M}{r}\right)^2 \left[1 + \left(\frac{\mathscr{L}}{r} - \omega_B r\right)^2\right] \,, \tag{24}$$

where $\mathscr{L}$ is the specific angular momentum of charged particle and it can be shifted as $\mathscr{L} \to \mathscr{L} + \omega_B M^2$, and ω_B is the magnetic parameter defined as $\omega_B = qB/2m$.

Our analyses show that that in the presence of the external magnetic field the effective potential is divergent at the large distance:

$$\lim_{r\to\infty} V(r) = \infty, \tag{25}$$

In the previous section, it was noted that the magnetic field solution was derived near the black hole. This allows us to safely use the effective potential in (24) for analyzing the orbit of a charged particle in the vicinity of the black hole.

By imposing the conditions $\dot{r} = \ddot{r} = 0$, the critical values of the specific energy and specific angular momentum for the charged particle can be determined as

$$\mathscr{E} = \frac{(r-M)^{3/2}\sqrt{r - 2M - 2Kr\omega_B + 2r^2(r-M)\omega_B^2}}{r(r-2M)} \,, \tag{26}$$

$$\mathscr{L} = \frac{r(K - Mr\omega_B)}{r - 2M} \,. \tag{27}$$

where $K = \sqrt{M(r-2M) + r^2(r-M)^2\omega_B^2}$. The stationary points of the specific energy and specific angular momentum in Eqs. (26) and (27) indicate the location of the MSCO for a charged particle in the BBMB spacetime with an asymptotic magnetic field. Careful numerical analysis shows that the MSCO position $r_{\rm ms}$ for both positively and negatively charged particles decrease in the presence of an external magnetic field. Figure 5 demonstrates the dependence of the MSCO position on the magnetic parameter ω_B for the charged particle in both BBMB and Schwarzschild spacetimes. As one can see in the plot, the MSCO position for the positively charged particle reaches the black hole's horizon in both metrics, respectively. However, for negatively charged particle the MSCO position is located a bit far from the horizon of the black hole as shown in Fig. 5. In Fig. 6 we show dependence of the energy efficiency of positively and negatively charged particles in both BBMB and Schwarzschild spacetimes. Our numerical calculations reveal that the energy efficiency for positively charged particles reaches approximately $\sim$ 100% in the BBMB spacetime and $\sim$ 99.9% in the Schwarzschild spacetime, but never reaches 100%. For negatively charged particles, the energy efficiency reaches up to around $\sim$ 33% in the BBMB spacetime and $\sim$ 27% in the Schwarzschild spacetime.

3.3 Charged accreting matter on to black hole

In this subsection, we examine a basic toy model of a thin accretion disk. We assume that the accreting matter around the black hole consists of charged particles and ions. With this setup, we can perform similar calculations to those conducted in the previous section. The measurable quantities for a charged particle, specific energy, angular momentum and specific angular velocity in the presence of an asymptotically uniform magnetic field can be expressed as

$$\mathscr{E} = -\frac{g_{tt}}{\sqrt{-g_{tt} - \Omega^2 g_{\phi\phi}}} \,, \tag{28}$$

$$\mathscr{L} = \frac{g_{\phi\phi}}{\sqrt{-g_{tt} - \Omega^2 g_{\phi\phi}}} - \frac{q}{m} A_\phi \,, \tag{29}$$

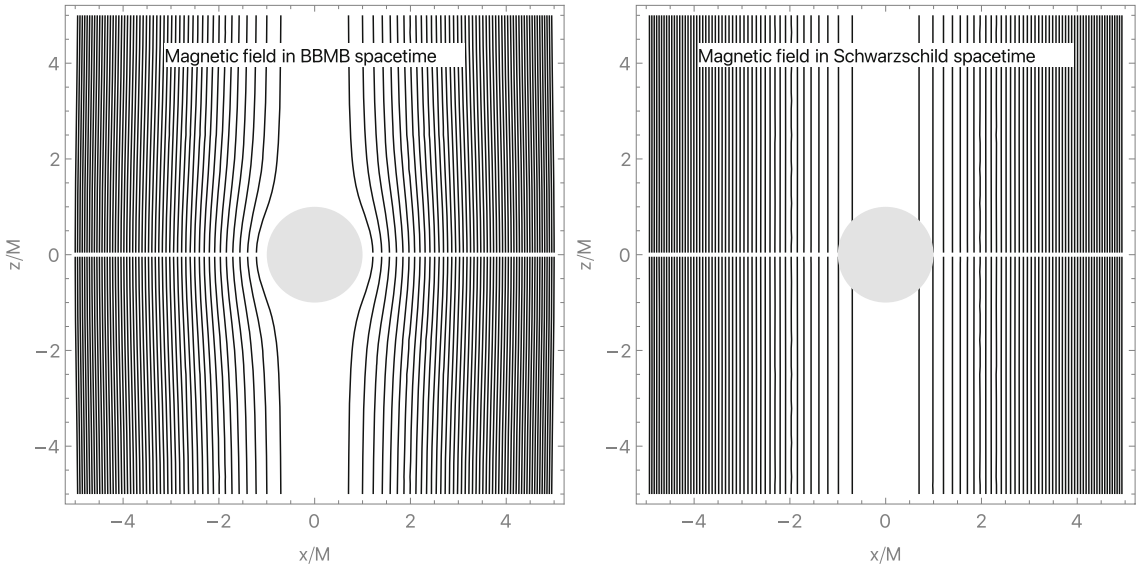

Fig. 4 The magnetic field lines in the vicinity of BBMB and Schwarzschild black holes in (x/M, z/M) plane for the magnetic field strength of 10^4G

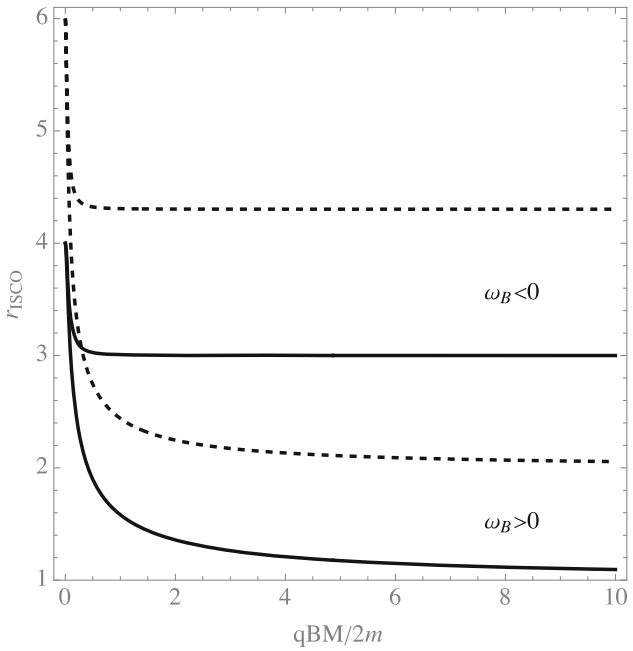

Fig. 5 Dependence of the MSCO radii for for positively and negatively charged particles in the BBMB spacetime (solid line) and Schwarzschild spacetime (dashed line) from the magnetic coupling parameter ω_B

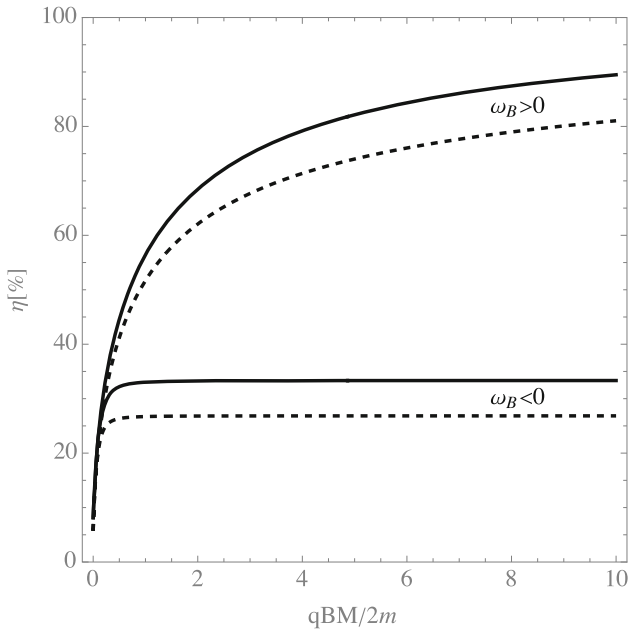

Fig. 6 Dependence of the energy efficiency for for positively and negatively charged particles in the BBMB spacetime (solid line) and Schwarzschild spacetime (dashed line) from the magnetic coupling parameter ω_B

$$\frac{\partial_r g_{tt} + \Omega^2 \partial_r g_{\phi\phi}}{\sqrt{-g_{tt} - \Omega g_{\phi\phi}}} = -\frac{2q}{m}\Omega^2 F_{r\phi}. \tag{30}$$

Analytical calculations for the radiant energy and temperature of a thin disk are quite challenging in the presence of a magnetic field. Therefore, we rely on numerical methods to determine the radial dependence of these key quantities. Figure 7 shows the radial dependence of the radiant energy and temperature of the thin disk surrounding the BBMB black hole. The results indicate that the external magnetic field significantly increases both quantities. Another noteworthy finding is that, for negative values of the magnetic parameter, the profiles of radiant energy and temperature are noticeably narrower compared to those for positive values of the magnetic parameter. This suggests that the distribution of neg-

ative particles in this ionized thin accretion model is more concentrated along the radial distance.

3.4 Synchrotron radiation

We now concentrate on investigating synchrotron radiation from a relativistic charged particle near a magnetized BBMB black hole. According to Reference [10], the expression for the four-momentum loss of the accelerated test particle can be written as

$$\frac{dP^{\alpha}}{d\lambda} = \frac{2q^4}{3m^2} w_{\beta} w^{\beta} \dot{x}^{\alpha} \,, \tag{31}$$

where λ is an afine parameter, w^{α} is the four-acceleration of charged particle in the presence of the asymptotic uniform magnetic field defined as $w^{\alpha} = \dot{x}^{\beta} \nabla_{\beta} \dot{x}^{\alpha}$ and it is always orthogonal to the four-velocity of particle i.e. $w_{\alpha} \dot{x}^{\alpha} \equiv 0$. It is well-known that an accelerated relativistic charged particle emits electromagnetic radiation. We now concentrate on the radiation emitted by an accelerated charged particle orbiting a black hole. The radiation spectrum of relativistic charged particle in curved spacetime can be expressed as [10,15]

$$I = -\frac{dP_{\alpha}}{d\lambda} \dot{x}^{\alpha} = \frac{2q^4}{3m^2} w_{\beta} w^{\beta} \,, \tag{32}$$

For simplicity, we consider the motion of charged particle in stable circular orbit with $\dot{x}^{\alpha} = \dot{t}(1, 0, 0, \Omega)$ to analyze the behavior of the radiation spectrum. Since the velocity and acceleration of the particle are orthogonal to each other, i.e., $w_{\alpha} \dot{x}^{\alpha} \equiv 0$, the four-acceleration of the particle can be expressed as

$$w^{\alpha} = (0, w_r, w_{\theta}, 0) = \frac{q\Omega}{\sqrt{-g_{tt} - \Omega^2 r^2}} (0, F_{r\phi}, F_{r\phi}, 0) \,, \tag{33}$$

and the intensity of charged particle in the presence of the eternal magnetic field reads

$$I = -\frac{2q^4}{3m^2} \frac{\Omega^2}{g_{tt} + \Omega^2 g_{\phi\phi}} (g^{rr} F_{r\phi} + g^{\theta\theta} F_{\theta\phi}^2) \,. \tag{34}$$

Similarly, one can also consider a more realistic scenario where a charged particle is falling into a black hole with the four-velocity $\dot{x}^{\alpha} = \dot{t}(1, u, 0, \omega)$, where $u = dr/dt$ is the radial velocity and $\omega = d\phi/dt$ is the angular velocity of the particle. In this case, from the condition $w_{\alpha} \dot{x}^{\alpha} = 0$, it follows that the radial acceleration of the charged particle vanishes ($w_r = 0$); however, vertical acceleration should still be present ($w_{\theta} \neq 0$). Finally, the intensity of radiation from the charged particle can be expressed as

$$I = -\frac{2q^4}{3m^2} \frac{g^{\theta\theta} F_{\theta\phi}^2 \omega^2}{g_{tt} + g^{rr} u + \omega^2 g_{\phi\phi}} . \tag{35}$$

4 Conclusions

We have extended the Novikov–Thorne model to analyze the thermal properties of thin accretion disks in BBMB spacetime, comparing them with those in Schwarzschild spacetime. Our study reveals that while the overall structure and

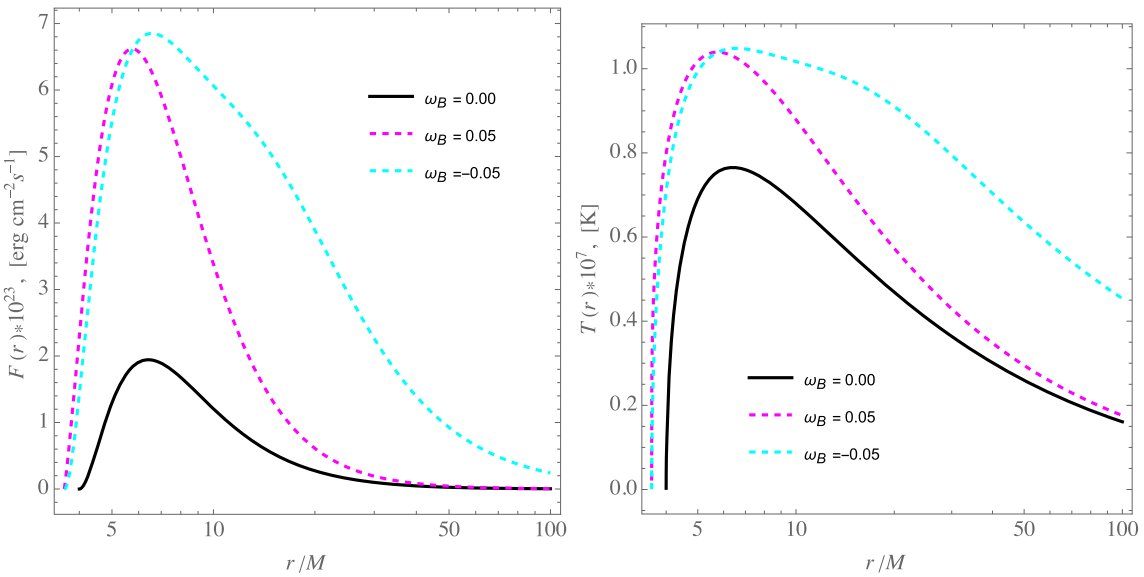

Fig. 7 Left panel: The profile of the radiant energy flux (left panel) and temperature (right panel) of the thin disk in the BBMB spacetime (solid line) and in the Schwarzschild spacetime (dashed line) for the value of accretion rate $\dot{\mathscr{M}} = 0.1 \dot{\mathscr{M}}_{\rm Edd}$

behavior of the accretion disks are similar in both spacetimes, the BBMB spacetime leads to a higher radiant energy flux and disk temperature near the black hole. Additionally, the radiative energy efficiency is slightly higher in the BBMB spacetime than in the Schwarzschild case. These differences suggest that observations of accretion disk spectra, particularly in the high-frequency X-ray region, could provide insights into the underlying spacetime geometry and help distinguish between these two gravitational theories.

We have explored the motion of charged particles within the BBMB spacetime under the influence of an external magnetic field. We considered an accretion disk composed predominantly of charged particles and derived the equations governing their motion in this curved spacetime. The analysis of the magnetic field configuration revealed that the magnetic field lines near the BBMB black hole extend more uniformly compared to the Schwarzschild spacetime, due to the additional term in the metric function. The effective potential for charged particle motion indicated divergence at large distances, confirming that the magnetic field significantly influences particle dynamics close to the black hole. The positions of the marginally stable circular orbits (MSCOs) for both positively and negatively charged particles were found to decrease with the presence of an external magnetic field. Positively charged particles showed MSCOs reaching the event horizon, while negatively charged particles' MSCOs remained slightly distant.

Furthermore, the study demonstrated that the energy efficiency of particle accretion is higher for positively charged particles, with the maximum efficiency reaching approximately $\sim 100\%$ in the spacetime of the magnetized BBMB black hole and nearly $\sim 99.9\%$ in the spacetime of the magnetized Schwarzschild black hole. Conversely, negatively charged particles exhibited lower energy efficiency, with maximum values around $\sim 33.2\%$ and $\sim 27\%$ in the BBMB and Schwarzschild spacetime, respectively. These findings underscore the complex interplay between magnetic fields and spacetime geometry in determining the dynamics of charged particles around black holes.

We also explored a simple toy model of a thin accretion disk around the BBMB black hole, assuming that the accreting matter consists of charged particles and ions. We derived the measurable quantities such as specific energy, angular momentum, and specific angular velocity for a charged particle in the presence of an asymptotically uniform magnetic field. The findings showed that the external magnetic field significantly changes both radiant energy and temperature. Additionally, for negative magnetic parameters, the profiles of these quantities are more narrowly distributed, indicating a more concentrated distribution of negative particles along the radial distance in the ionized thin accretion disk.

Finally, we studied synchrotron radiation generated by the acceleration of charged particles near the magnetized BBMB black hole. We have derived explicit formulas for the intensity of radiation emitted by relativistic charged particles, accelerated by electromagnetic forces (both Coulomb and Lorentz), in the vicinity of the magnetized black hole. Numerical results indicate that the radiation intensity from these accelerated particles near the magnetized black hole is on the order of $\sim 10^{35}$ erg/s. Additionally, a significant finding reveals that a charged particle falling radially towards the black hole experiences vertical acceleration, which implies it can emit electromagnetic radiation in this scenario. Further interesting research involves studying the acceleration of charged particles around a rotating magnetized black hole (magnetized Kerr black hole), particularly focusing on how the black hole's rotation and the external magnetic field affect the synchrotron radiation emitted by these accelerated particles. Investigations on these aspects are currently ongoing.

Data Availability Statement My manuscript has no associated data. [Authors' comment: No data has been associated in this article.]

Code Availability Statement My manuscript has no associated code/software. [Authors' comment: Code/Software sharing not applicable to this article as no code/software was generated or analysed during the current study.]

Funded by SCOAP[3].

References

1. M. Kološ, M. Shahzadi, A. Tursunov, https://doi.org/10.48550/arXiv.2304.13603. arXiv e-prints arXiv:2304.13603 (2023)
2. M. Kološ, M. Shahzadi, in *Proceedings of RAGtime 23-25: Workshops on Black Holes and Neutron Stars*, ed. by Z. Stuchlik, G. Torok, V. Karas, D. Lancova (2023), pp. 21–27
3. M. Kolos, D. Bardiev, B. Juraev, in *RAGtime 20-22: Workshops on Black Holes and Neutron Stars. Proceedings of RAGtime 20-22. Edited by Z. Stuchlík*, ed. by Z. Stuchlík, G. Török, V. Karas (2020), pp. 145–152
4. J. Vrba, A. Abdujabbarov, M. Kološ, B. Ahmedov, Z. Stuchlík, J. Rayimbaev, PRD **101**(12), 124039 (2020). https://doi.org/10.1103/PhysRevD.101.124039
5. A. Tursunov, Z. Stuchlík, M. Kološ, PRD **93**(8), 084012 (2016). https://doi.org/10.1103/PhysRevD.93.084012
6. Z. Stuchlík, M. Kološ, Eur. Phys. J. C **76**, 32 (2016). https://doi.org/10.1140/epjc/s10052-015-3862-2

7. A. Davlataliev, B. Narzilloev, I. Hussain, A. Abdujabbarov, B. Ahmedov, Eur. Phys. J. C **84**(7), 694 (2024). https://doi.org/10.1140/epjc/s10052-024-13039-3
8. A.N. Aliev, N. Özdemir, MNRAS **336**(1), 241 (2002). https://doi.org/10.1046/j.1365-8711.2002.05727.x
9. V.P. Frolov, A.A. Shoom, PRD **82**(8), 084034 (2010). https://doi.org/10.1103/PhysRevD.82.084034
10. L.D. Landau, E.M. Lifshitz, *The Classical Theory of Fields, Course of Theoretical Physics*, vol. 2 (Elsevier Butterworth-Heinemann, Oxford, 2004)
11. Z. Stuchlík, M. Kološ, A. Tursunov, D. Gal'tsov, Universe **10**(6), 249 (2024). https://doi.org/10.3390/universe10060249
12. A. Tursunov, M. Kološ, Z. Stuchlík, D.V. Gal'tsov, ApJ **861**(1), 2 (2018). https://doi.org/10.3847/1538-4357/aac7c5
13. A. Tursunov, M. Kološ, in *RAGtime 17-19: Workshops on Black Holes and Neutron Stars* (2017), pp. 211–221
14. A.A. Shoom, PRD **92**(12), 124066 (2015). https://doi.org/10.1103/PhysRevD.92.124066
15. B. Turimov, M. Boboqambarova, B. Ahmedov, Z. Stuchlík, Eur. Phys. J. Plus **137**(2), 222 (2022). https://doi.org/10.1140/epjp/s13360-022-02390-7
16. B. Turimov, A. Nosirov, A. Abdujabbarov, Phys. Dark Univ. **42**, 101375 (2023). https://doi.org/10.1016/j.dark.2023.101375
17. B. Turimov, H. Alibekov, P. Tadjimuratov, A. Abdujabbarov, Phys. Lett. B **843**, 138040 (2023). https://doi.org/10.1016/j.physletb.2023.138040
18. Event Horizon Telescope Collaboration, K. Akiyama et al., Astrophys. J. Lett. **875**(1), L1 (2019). https://doi.org/10.3847/2041-8213/ab0ec7
19. C. Bambi, K. Freese, S. Vagnozzi, L. Visinelli, Phys. Rev. D **100**(4), 044057 (2019). https://doi.org/10.1103/PhysRevD.100.044057
20. C. Bambi, Rev. Mod. Phys. **89**(2), 025001 (2017). https://doi.org/10.1103/RevModPhys.89.025001
21. C. Bambi, Mod. Phys. Lett. A **26**(33), 2453 (2011). https://doi.org/10.1142/S0217732311036929
22. M. Ghasemi-Nodehi, C. Chakraborty, Q. Yu, Y. Lu, Eur. Phys. J. C **81**(10), 939 (2021). https://doi.org/10.1140/epjc/s10052-021-09696-3
23. G. Erez, N. Rosen, Bull. Res. Council Israel **8F**, 47 (1959)
24. R. Genzel, F. Eisenhauer, S. Gillessen, Rev. Mod. Phys. **82**(4), 3121 (2010). https://doi.org/10.1103/RevModPhys.82.3121
25. A.M. Ghez, S. Salim, N.N. Weinberg, J.R. Lu, T. Do, J.K. Dunn, K. Matthews, M.R. Morris, S. Yelda, E.E. Becklin, T. Kremenek, M. Milosavljevic, J. Naiman, Astrophys. J. **689**(2), 1044 (2008). https://doi.org/10.1086/592738
26. F. Tamburini, B. Thidé, M. Della Valle, MNRAS **492**(1), L22 (2020). https://doi.org/10.1093/mnrasl/slz176
27. C. Bambi, Astrophys. J. **761**(2), 174 (2012). https://doi.org/10.1088/0004-637X/761/2/174
28. C. Bambi, Phys. Rev. D **87**(2), 023007 (2013). https://doi.org/10.1103/PhysRevD.87.023007
29. N.I. Shakura, R.A. Sunyaev, Astron. Astrophys. **500**, 33 (1973)
30. J.E. Pringle, Ann. Rev. Astron. Astrophys. **19**, 137 (1981). https://doi.org/10.1146/annurev.aa.19.090181.001033
31. M.A. Abramowicz, P.C. Fragile, Living Rev. Relativ. **16**(1), 1 (2013). https://doi.org/10.12942/lrr-2013-1
32. I.D. Novikov, K.S. Thorne, in *Black Holes (Les Astres Occlus)* (1973), pp. 343–450
33. D.N. Page, K.S. Thorne, Astrophys. J. **191**, 499 (1974). https://doi.org/10.1086/152990
34. K.S. Thorne, Astrophys. J. **191**, 507 (1974). https://doi.org/10.1086/152991
35. J.P. Luminet, Astron. Astrophys. **75**, 228 (1979)
36. Y. Mizuno, Z. Younsi, C.M. Fromm, O. Porth, M. De Laurentis, H. Olivares, H. Falcke, M. Kramer, L. Rezzolla, Nat. Astron. **2**, 585 (2018). https://doi.org/10.1038/s41550-018-0449-5
37. M. Heydari-Fard, S. Ghassemi Honarvar, M. Heydari-Fard, MNRAS **521**(1), 708 (2023). https://doi.org/10.1093/mnras/stad558
38. M. Heydari-Fard, M. Heydari-Fard, H.R. Sepangi, Eur. Phys. J. C **81**(5), 473 (2021). https://doi.org/10.1140/epjc/s10052-021-09266-7
39. M. Heydari-Fard, H.R. Sepangi, Phys. Lett. B **816**, 136276 (2021). https://doi.org/10.1016/j.physletb.2021.136276
40. M. Heydari-Fard, M. Heydari-Fard, H.R. Sepangi, Eur. Phys. J. C **80**(4), 351 (2020). https://doi.org/10.1140/epjc/s10052-020-7911-0
41. G. Sen, C. Chakraborty, S. Bhattacharyya, D. Maity, S. Chakrabarti, S. Das, https://doi.org/10.48550/arXiv.2408.03270. arXiv e-prints arXiv:2408.03270 (2024)
42. Y. Shen, B. Chen, JCAP **2024**(7), 063 (2024). https://doi.org/10.1088/1475-7516/2024/07/063
43. P.B. Ivanov, V.V. Zhuravlev, MNRAS **528**(1), 337 (2024). https://doi.org/10.1093/mnras/stae005
44. C. Tiede, in *American Astronomical Society Meeting Abstracts*, vol. 241 (2023), p. 435.05
45. T.Y. He, Z. Cai, R.J. Yang, Eur. Phys. J. C **82**(11), 1067 (2022). https://doi.org/10.1140/epjc/s10052-022-11037-x
46. S. Guo, G.R. Li, E.W. Liang, Class. Quantum Gravity **39**(13), 135004 (2022). https://doi.org/10.1088/1361-6382/ac6fa8
47. C. Liu, S. Yang, Q. Wu, T. Zhu, JCAP **2022**(2), 034 (2022). https://doi.org/10.1088/1475-7516/2022/02/034
48. O.S. Stashko, V.I. Zhdanov, A.N. Alexandrov, PRD **104**(10), 104055 (2021). https://doi.org/10.1103/PhysRevD.104.104055
49. G. Gyulchev, P. Nedkova, T. Vetsov, S. Yazadjiev, Eur. Phys. J. C **81**(10), 885 (2021). https://doi.org/10.1140/epjc/s10052-021-09624-5
50. L.G. Collodel, D.D. Doneva, S.S. Yazadjiev, APJ **910**(1), 52 (2021). https://doi.org/10.3847/1538-4357/abe305
51. S. Faraji, E. Hackmann, https://doi.org/10.48550/arXiv.2010.02786. arXiv e-prints arXiv:2010.02786 (2020)
52. A. Habibi, S. Abbassi, APJ **887**(2), 256 (2019). https://doi.org/10.3847/1538-4357/ab5793
53. J. Li, X. Cao, APJ **872**(2), 149 (2019). https://doi.org/10.3847/1538-4357/ab0207
54. P.L. Shaw, P.C. Fragile, B. Mishra, in *American Astronomical Society Meeting Abstracts #233*, vol. 233 (2019), p. 348.04
55. M. Čemeljić, V. Parthasarathy, W. Kluźniak, https://doi.org/10.48550/arXiv.1812.09132. arXiv e-prints arXiv:1812.09132 (2018)
56. S. Kenzhebayeva, S. Toktarbay, A. Tursunov, M. Kološ, PRD **109**(6), 063005 (2024). https://doi.org/10.1103/PhysRevD.109.063005
57. B. Turimov, B. Ahmedov, Symmetry **15**(10), 1858 (2023). https://doi.org/10.3390/sym15101858
58. B. Turimov, O. Rahimov, B. Ahmedov, Z. Stuchlík, K. Boymurodova, Int. J. Mod. Phys. D **30**(5), 2150037–407 (2021). https://doi.org/10.1142/S0218271821500371
59. N.M. Bocharova, K.A.S. Bronnikov, V.N. Mel'Nikov, Vestn. Mosk. Un-Ta. Fiz. **11**, 706 (1970)
60. J.D. Bekenstein, Ann. Phys. **82**, 535 (1974). https://doi.org/10.1016/0003-4916(74)90124-9
61. R.M. Wald, Phys. Rev. D **10**(6), 1680 (1974). https://doi.org/10.1103/PhysRevD.10.1680